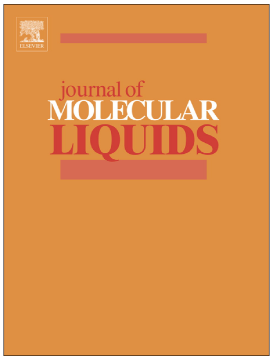

Photoacid as ICT probe for ground state proton transfer process from solute to solvents

Sumit Kumar Panja

PII: S0167-7322(19)35448-0

DOI: https://doi.org/10.1016/j.molliq.2019.112194

Reference: MOLLIQ 112194

To appear in: *Journal of Molecular Liquids*

Received date: 1 October 2019

Revised date: 19 November 2019

Accepted date: 21 November 2019

Please cite this article as: S.K. Panja, Photoacid as ICT probe for ground state proton transfer process from solute to solvents, *Journal of Molecular Liquids*(2019), https://doi.org/10.1016/j.molliq.2019.112194

Photoacid as ICT Probe for Ground State Proton Transfer Process from Solute to Solvents

Sumit Kumar Panja,*

Department of Chemistry, Uka Tarsadia University, Maliba Campus, Gopal Vidyanagar,Bardouli, Mahuba Road, Surat-394350, Gujrat, India

KEYWORDS: Photoacid, Solute-solvent Interaction, Ground State Proton Transfer (GSPT), Intramolecular Charge Transfer (ICT), Donor-acceptor.

Abstract: In present work, 2-(4-Hydroxybenzylidene)malononitrile (HyDC) acts as a photoacid and intramolecular charge transfer (ICT) probe for monitoring solvent specific ground state proton transfer (GSPT) process from solute to solvents. Presence of electron accepting group in HyDC, photoacidic nature and GSPT process are enhanced and observed by UV-vis spectroscopy. HyDC shows microsolvation behavior with protic solvents at ground state. Microsolvated clusters of HyDC with solvents are formed and supported by experimental and theoretical results.

Introduction

Intermolecular interactions involving aromatic rings play an important role not only on chemical and biological recognition processes but also in rational designs of drugs and other new functional materials [1]. Therefore, study of fundamental intermolecular interactions is of great importance for designing the new valuable materials and better understanding mechanism of cluster formation in solution as well [2]. Among several intermolecular interactions, H-bonding interaction has been extensively studied on a variety of small molecular clusters to probe the solvation phenomena, as solvation effects plays an important role in defining structural and functional aspects of biological macromolecules [2-3].

So, significant contribution and most important characteristic feature of intermolecular interaction between solvent and solute are described by intermolecular hydrogen bonding interaction [4-5]. Generally, photoacid exhibits microsolvation behavior with protic solvent via intermolecular hydrogen bonding interactions. Photosensitive nature of photoacids can be explained in terms of difference in pK_a value of ground and excited states [6]. The excited state pK_a^* of a photoacid is generally determined from the Förster cycle, based on absorption and emission data [7]. Photoacids undergo significant enhancement in their acidity upon electronic excitation [8]. These intermolecular hydrogen bonding interaction and degree of photoacidity of photoacids lead to ground state proton transfer process from solute to solvent [6]. Significant change in acidity of photoacids make them an ideal system and can be used for probing solute-solvent interactions and ground state proton transfer process from solute to solvent [8-9]. Studies on microhydration of photoacids can provide better insight into hydration process and proton transfer phenomena, considering a solute molecule surrounded by a small number of H_2O solvent molecule [10]. Electronic structure calculations of such a hydrated cluster of photoacid can help to have molecular level understanding about the hydration process [11-12]. Photoacids can be used as molecular probe for determining the structural transitions of proteins under various conditions [13-14]. Water accessibility in biological surfaces can also be probed using photo acids [15].

Phenol is the simplest photoacid which involves the aromatic rings and works as a chromophore in aromatic amino acid (e.g. tyrosine) [16-17]. Interaction of phenol with interacting solvent molecule can be employed as model system for studying microsolvated phenol clusters [3, 10, 18]. Theoretical calculations have been reported to explain excited state proton transfer process from phenol to solvent [12]. It is also reported that enhancement of charge transfer process (ICT) is observed with increasing acidity of photoacid and in presence of weak or strong bases [19-20]. Inhomogeneous clusters include water/alcohol [21-22], water/aromatic alcohol [23-26], alcohol/aromatic alcohol [27-30], and other more complicated related systems are explored using infrared (IR) and/or ultraviolet (UV) spectroscopic methods [31-32]. Even subtle perturbations caused by the hydrogen bonding interactions in these clusters result in redshifts of O−H vibrational stretching energies or change the π−π* electronic transition energies of aromatic groups [33-34]. These studies indicate that solvation of photoacid can have a dramatic effect on electronic properties of solute molecule. Experimental and theoretical analysis of solute-solvent interaction provide greater insight into nature H-bonding interactions [35-36].

Further, Knoevenagel product is obtained from well-known carbon-carbon bond-forming reaction, it is also widely used in the chemical, pharmaceutical and perfume industries [37]. The reaction is also well known for the synthesis of a large variety of intermediates useful in the manufacturing of top selling drugs (such as atorvastatin, pioglitazone, AMG 837, pregabalin, lumefantrine, entacapone) in the world [38-39]. Recently, Knoevenagel product is used for evidence of CT complex formation between a probe and unreacted methylimidazole in imidazolium cation based ionic liquids [40].

In present work, we have shown that 2-(4-Hydroxybenzylidene)malononitrile (HyDC, Chart 1) is acts as photoacid and used as ICT probe for monitoring ground state proton transfer (GSPT) process based on solute-solvent interaction.

Chart 1: Structural Formula and Abbreviation for Investigated System

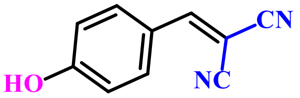

2-(4-Hydroxybenzylidene)malononitrile
(HyDC)

Experimental Section

Chemicals and Synthesis: All materials were of analytical grade and procured from Sigma Aldrich including solvents for the synthesis (ultrapure water, acetonitrile, dichloromethane, ethanol) and $CDCl_3$ for the NMR experiments.

General Procedure

4-Hydroxybenzaldehyde (1 mmol) and malononitrile (1.01 mmol), catalyst (0.05 mmol) were taken in a round bottom flask stirred at room temperature for the stipulated period of time till the completion of the reaction (monitored by TLC). After completion of the reaction, solid precipitated separated out, filtered and washed with water (3x10 mL) followed by ethanol (3x10 mL), dried in high vacuum to afford NMR pure product [40].

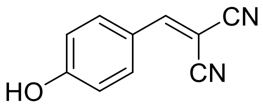

Characterization of HyDC: State: Solid; Colour: White; Melting Point: 190.0 °C; FTIR (KBr, cm^{-1}): 3350, 3330, 3090, 3070, 3035, 2937, 2228, 1555, 1565, 1495; ^{1}H-NMR (300 MHz, $CDCl_3$): δ (ppm) 10.38 (s, 1H), 7.82 (d, J = 8.7 Hz, 2H), 7.65 (s, 1H), 6.95 (d, J = 8.7 Hz, 2H); ^{13}C-NMR (75 MHz, $CDCl_3$): δ (ppm) 163.2, 162.6, 154.6, 133.8, 132.0, 128.6, 122.8, 116.3, 115.8, 97.5, 62.0.

Instrumentation

Steady State UV-Vis and Fluorescence Measurement: Steady state Uv-Vis and fluorescence spectral measurements were done at $\sim 10^{-5}$ to 10^{-6} M concentrations range. The steady state absorption spectra were recorded on Hitachi UV-vis U-3501 spectrophotometer. The fluorescence spectra were recorded on a Perkin-Elmer LS55 fluorescence spectrophotometer equipped with a 10 mm quartz cell and a thermostat bath.

Infrared Spectroscopy: FTIR-8900 spectrophotometer was used for recording FTIR in the 4000-400 cm^{-1} region using KBr.

Raman Spectroscopy. Fourier transform Raman spectra were acquired on a Vertex 70-RAM II Bruker FT-RAMAN spectrometerwith a Nd:YAG laser (wavelength 1064 nm, maximum power

1.5 W). The instrument is equipped with a liquid-nitrogen cooled Ge detector.The spectra (200-2500 cm^{-1}) were collected with 1 cm^{-1} nominal resolution by co-adding 128 scans.

Quantum Chemical Calculation:

DFT calculations with a hybrid functional CAM-B3LYP (Becke's three parameter hybrid functional using the LYP correlation functional) at 6-311G (d, p) basis set were performed with the Gaussian 09W software package [42]. The Gaussian 09 suite of programs was used for all the computations, and the GaussView 5.1 program was used to visualize the structures [42]. The electronic absorption spectra were calculated using the time-dependent density functional theory (TD-DFT) and CAM-B3LYP functional with 6-311G++ (d, p) basis and polarizable continuum model (PCM) with CAN, H_2O, EtOH and DMSO as solvent. DFT calculations were employed to calculate the optimized energies and to compute possible different geometries of solute-solvent clusters using CAM-B3LYP functional with 6-311G++ (d, p) basis and polarizable continuum model (PCM) with ACN, H_2O, EtOH and DMSO as solvent.

Results and Discussion

UV-Visible studies of HyDC in different solvents

UV-Vis spectra of HyDC molecule are measured in different solvents and normalized UV-Vis spectrum of HyDC is shown in Figure 1. From detailed analysis of UV-Vis spectra, intramolecular charge transfer (ICT) band and $\pi \rightarrow \pi^*$ electronic transition band are observed for HyDC in solution. In polar aprotic solvent strong $\pi \rightarrow \pi^*$ electronic transition is observed at 347 nm. But in polar protic solvent, strong $\pi \rightarrow \pi^*$ electronic transition (at 347 nm) along with a weak ICT process at 430 nm also observed. Intensity of ICT band varies depending upon nature and polarity of solvent (Figure 1). Interesting factor is that molar extinction coefficient of ICT band is very low in ethanol but higher in 2-propanol, H_2O and DMSO (Figure 1). From above experimental results, it is clear that solute-solvent interaction is very specific and depends on nature of solvents.

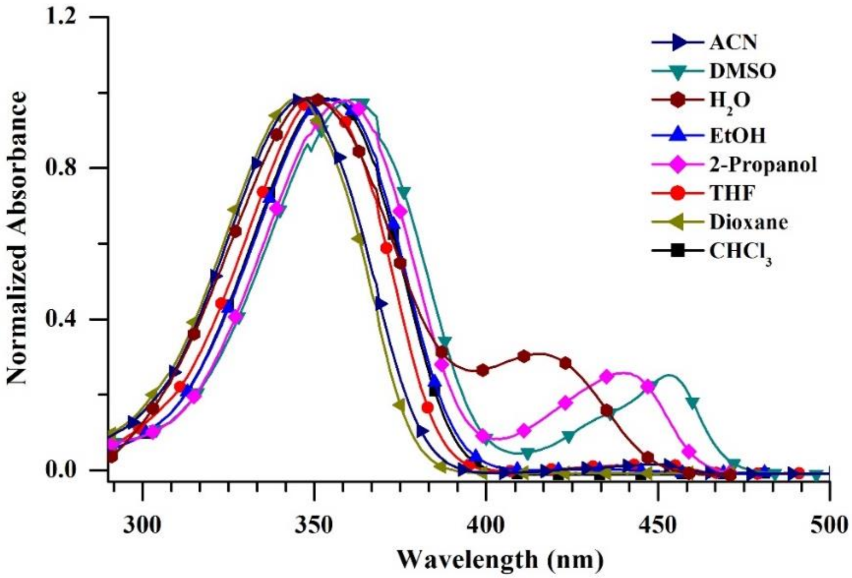

Figure 1: Normalized UV-Vis spectra of HyDC in different solvents

In ACN, UV-vis spectrum of HyDC is altered after gradually addition of H_2O (ESI-Figure 1). During experiment, absorption band at 343 nm is shifted to 348 nm after addition of H_2O from 0 ml to 0.6 ml along with appearance of new absorption band at 435 nm. Spectral shift is found to be 5 nm and presented in Figure 2. Further, normalized spectrum of above experiment is presented for better understanding the experimental facts (in Figure 2 and onset).

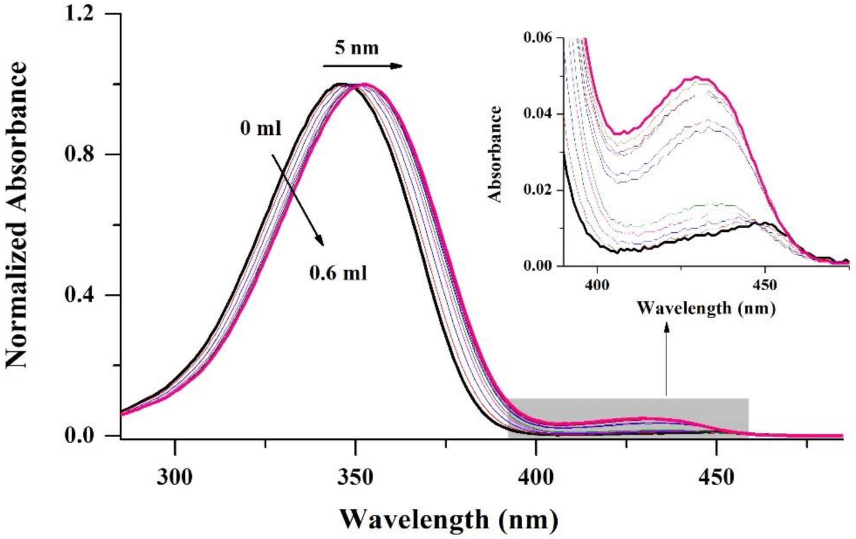

Figure 2: Normalized absorption spectra of HyDC in ACN after addition of H_2O (Conc:$1.1x10^{-6}$ M)

The appearance of new absorption band at 435 nm is due to specific HyDC-H_2O interaction. Similarly, strong solute-solvent interaction is observed in DMSO solvent (Figure 1and 3). As strong solute-solvent interaction is observed in DMSO and H_2O solvents at room temperature, (Figure 1, 3), effect of temperature on solute-solvent interaction in H_2O and DMSO solvents has been investigated by UV-vis study. Molar extinction coefficient of ICT band and $\pi \rightarrow \pi^*$ electronic band is not affected by temperature from 25 °C to 75 °C in DMSO (Figure 3). But molar extinction coefficient of ICT band increases and subsequently $\pi \rightarrow \pi^*$ electronic band decreases from 25 °C to 75 °C in H_2O (Figure 4). From above experimental results, it is clear that strong solute-solvent interaction is observed in DMSO and H_2O. The dissociation of solute-solvent complex by temperature is insignificant in DMSO but prominent in H_2O. The equilibrium between solute and solvent in solute-solvent complex is observed in H_2O due to alternation of orientation and intermolecular interaction by temperature.

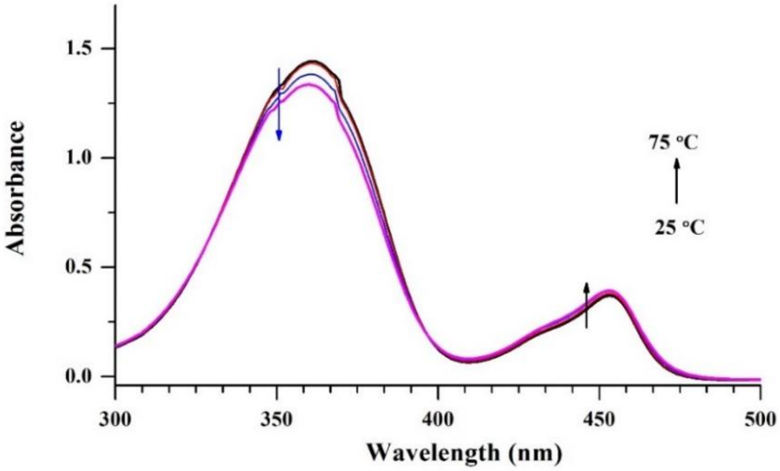

Figure 3: Temperature dependent UV-Vis spectra of HyDC in DMSO (Conc:1.1x10^{-6} M)

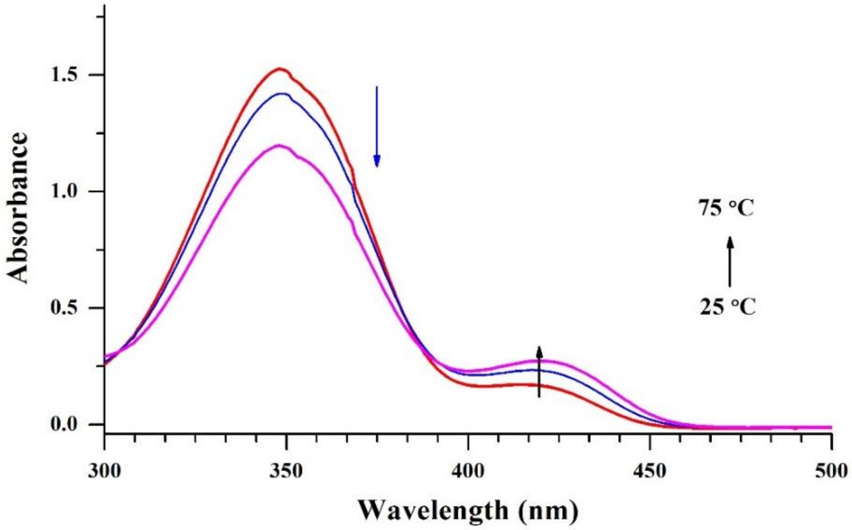

Figure 4: Temperature dependent UV-Vis spectra of HyDC in H_2O (Conc:1.1x10^{-6} M)

Further, effect of base on ICT process of HyDC is also investigated in ACN solvent. In presence of KOH, weak electron donor group (-OH) is converted to strong electron donating group (-O^-), results strong electron donor-acceptor system and strong ICT process is observed from strong electron donor to strong electron acceptor group. Initially, ICT process of HyDC is not observed in ACN due to weak electron donor group (-OH) but ICT process is enhanced after addition of KOH in ACN solvent (Figure 5).

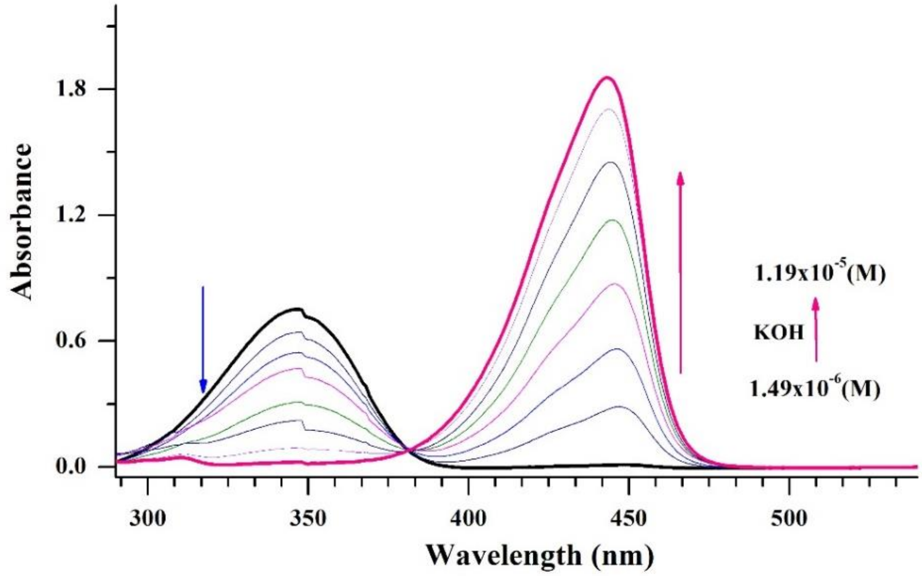

Figure 5: UV-Vis titration of HyDC with different KOH concentration in ACN

The ICT band is appeared at 443 nm and intensity of ICT band is enhanced by gradually addition of KOH and, but intensity of $\pi \rightarrow \pi^*$ band at 345 nm decreases significantly in ACN. Deprotonation of -OH group is taken place in presence base (KOH) and protonation of -O^{-} group in presence of TFA (tetrafluoro acetic acid) has been investigated by monitoring the relative intensity of ICT band. Deprotonated HyDC (-O^{-}) is formed linearly with addition of KOH in ACN which is similar observation from our similar previous work [43].

After completion of KOH addition, TFA solution (trifluoroacetic acid) is gradually added to previous solution containing KOH. Initially, after addition of TFA, change of intensity of ICT band is very high. But suddenly, it becomes very low after addition of TFA and (Figure 6). From these experimental results, formation of protonated HyDC (-O-H) from deprotonated HyDC (-O^{-}) becomes very fast at initial stage but later on it is formed at very slow rate due to presence of small amount of deprotonated HyDC in solution. Protonation process of HyDC anion is highly favorable and supported by experimental results.

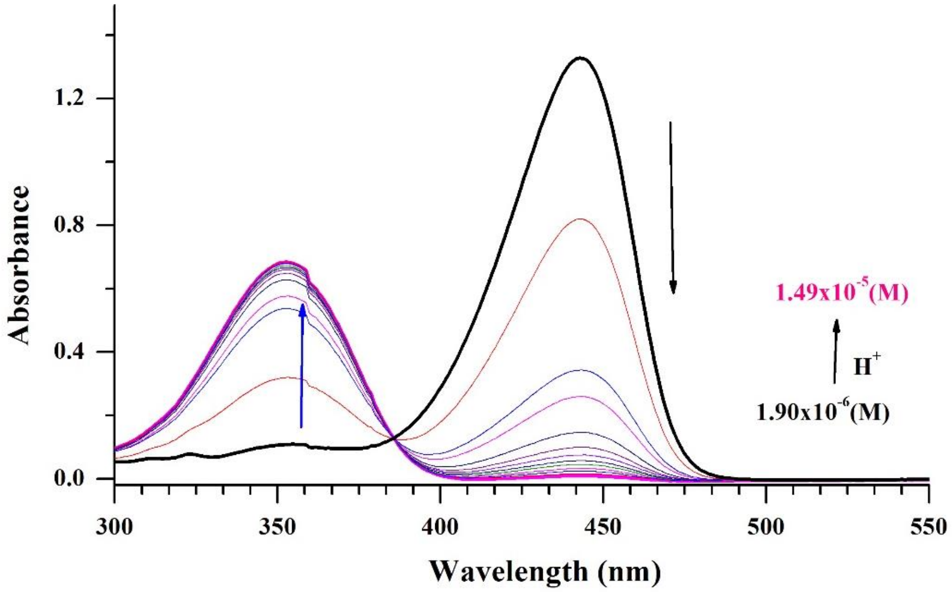

Figure 6: UV-Vis titration of KHyDC at different TFA concentrations in ACN

Further, Benesi-Hildebrand (B-H) method has been employed to determine dissociation constant (K_d) by UV-Vis spectroscopy [44]. The B-H plot is carried out at 443 nm for HyDC dissociation in ACN (ESI-equation 1). Linearity of B-H plot indicates that experimental result is acceptable for 1:1 system (ESI-Figure 2). Dissociation constant (K_d), intercept and slope are obtained from linear fit curve (Table 1 and ESI-Figure 2). The K_d value of HyDC is 2.59x10^4 cm^3 mol^{-1} at 443 nm in ACN. B-H plot is carried out at particular wavelength at 443 nm for formation of HyDC (ESI-Equation 2). The formation constant (K_f), intercept and slope are obtained from linear fit curve (Table 1 and ESI-Figure 3). The K_f value of HyDC formation is 7.15x105 cm^3 mol^{-1} at 443 nm in ACN.

Table 1: Experimental parameters for K_d and K_f of HyDC in ACN

K_d (dissociation constant) in ACN

Intercept (1/[A-Ao])	Slope (1/K [A-Ao])	χ^2	K ($cm^3\ mol^{-1}$)
0.11	$4.44x10^{-6}$	0.99	2.59 $x10^4$ (@443 nm
K_f (formation constant) in ACN			
0.71	$1.01x10^{-6}$	0.99	7.15 $x10^5$ (@443 nm

From above experimental results, it is clear that deprotonation and protonation process of HyDC in ACN are reversible by monitoring intensity alternation of ICT band (Figure 7) ICT band is observed from deprotonated HyDC molecule in solution and represents the population of deprotonated form in ACN.

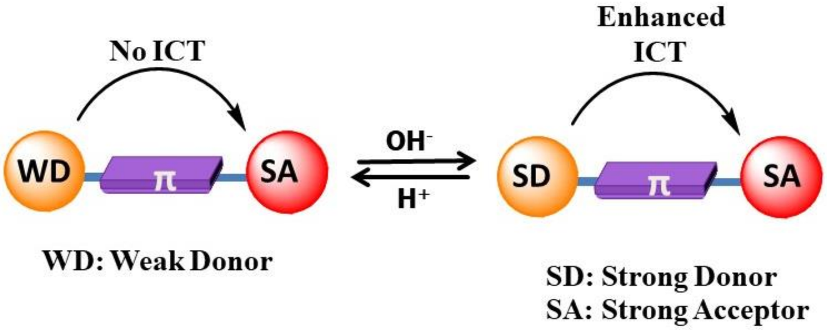

Figure 7: Schematic presentation of reversible ICT process

Deprotonated HyDC is only formed if proton from O-H bond of protonated HyDC is transferred to solvent via solute-solvent interaction. Depending upon solute-solvent interaction, intensity of ICT band population of deprotonated HyDC molecule is altered. From experimental observation by comparing the relative intensities of ICT bands, it is observed that solute-solvent interaction is weak in ACN solvent but strong in DMSO and H_2O solvents. Above results indicate that ground state proton transfer is occurring from solute (HyDC) to solvents. The degree of ground state proton transfer is observed from solute (HyDC) to solvents is higher in DMSO and H_2O compared to ACN.

From concentration dependent fluorescent experiment, self-quenching is observed in solvents (ESI-Figure 4-5). The self-quenching may happen due to intermolecular interactions and parallel arrangement of two dipole molecule in opposite charge site in solution.

Quantum Chemical Calculation

Microhydration at Ground State:

For optimization of geometry, DFT method is adopted using hybrid functional CAM-B3LYP (Becke's three parameter hybrid functional using the LYP correlation functional) at 6-311G++ (d, p) basis and polarizable continuum model (PCM) with respective solvents for individual solute-solvent cluster. At ground state, optimized geometry of HyDC is presented in figure 8a and ESI-figure 5. In optimized structure of HyDC, bond length of O-H bond is found to be 0.96 Å. For most stable conformer of HyDC with single DMSO molecule, H atom of -OH group from HyDC forms H-bond with O atom of the DMSO (Figure 8b). In optimized structure of HyDC-DMSO complex, bond length of O-H bond is found to be 1.00 Å which is longer than its optimized geometry and H-bonded H--DMSO distance is found to be 1.59Å. In HyDC-EtOH complex (1:1), the bond length of O-H bond is also found to be 0.99 Å which is longer than its optimized geometry and H-bonded H--EtOH distance is found to be 1.69Å (Figure 8c).

Similarly, with addition of a single H_2O molecule, most stable conformer of HyDC forms hydrogen bond between H-O group and O atom of H_2O molecule (Figure 8c). From optimized structure of HyDC-H_2O complex (1:1), bond length of O-H bond is 0.98 Å, which is shorter than HyDC-DMSO complex and longer than its optimized geometry and supported by previously reported work [45]. The H-bonded H--OH_2 distance is found to be 1.70 Å (Figure 8d). The O-H bond length of HyDC molecule increases to 1.00 Å (mono HyDC-DMSO complex) from 0.96 Å (HyDC alone) and the C-O bond length of HyDC decreases to 1.33 Å (mono HyDC-DMSO complex, HyDC-EtOH and HyDC-H_2O) from 1.35Å (HyDC alone). The H-bond distance between oxygen atom of O-H in HyDC and O atom of DMSO, EtOH and H_2O molecule is calculated to be 2.59 Å, 2.67 Å and 2.69 Å respectively.

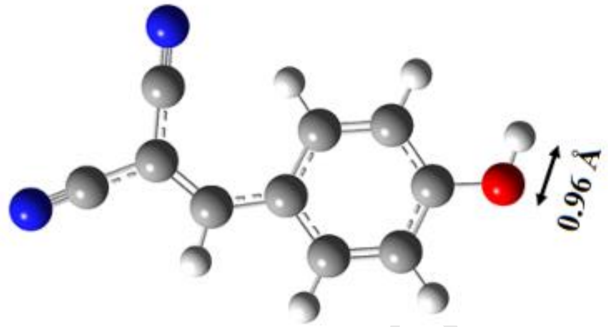

Figure 8a. Optimized structure of HyDC

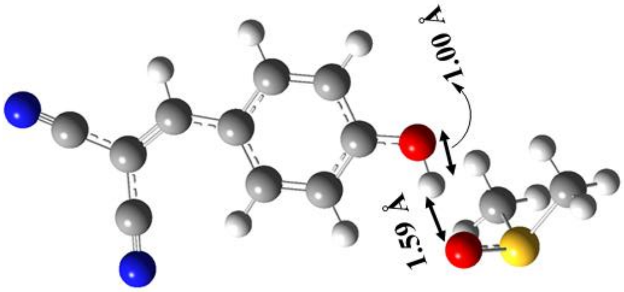

Figure 8b. Optimized structure of HyDC-DMSO complex

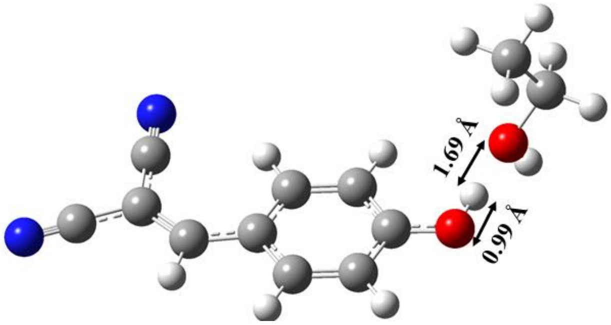

Figure 8c. Optimized structure of HyDC-EtOH complex

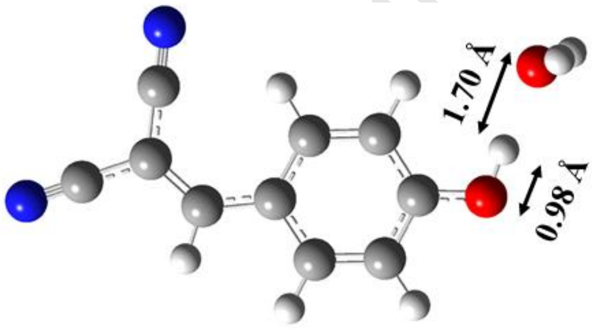

Figure 8d. Optimized structure of HyDC H_2O complex

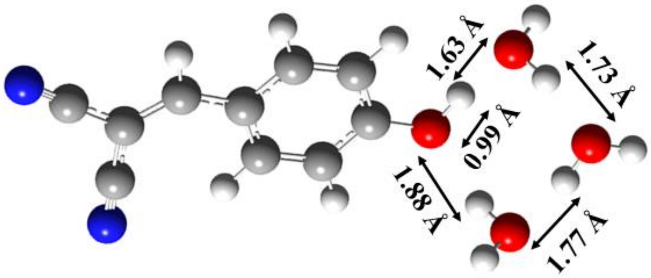

Figure 8e. Optimized structure of HyDC-$(H_2O)_3$ complex

With three H_2O molecules, most stable conformer (Figure 8e) shows that O-H bond of HyDC is hydrogen bonded to oxygen atom of one H_2O molecule and hydrogen atom of another H_2O

molecule formed with oxygen atom of O-H bond of HyDC. Third H_2O molecule forms H-bond to previous two H-bonded H_2O molecules with HyDC molecule in cyclic way (Figure 8e). Four H-bonding interaction sites in HyDC-$(H_2O)_3$ complex (1:3) is different and found to be different hydrogen bonding interaction energy from DFT calculation. The O−H and C−O bond lengths in most stable HyDC-$(H_2O)_3$ complex (1:3) is 0.99 and 1.33 Å respectively which has closed ring geometry [46-47]. Further, optimization of all solute-solvent clusters in gaseous phase and detailed information regarding bond lengths are presented in ESI-6a-6d.

From theoretical studies, the O-H bond length of HyDC molecule and internuclear distance via H-bonding interaction between oxygen atom of O-H in HyDC and O atom of DMSO, EtOH and H_2O molecule is different but the C-O bond length of HyDC is similar value for HyDC-solvent complex (1:1). From experimental UV-Vis results, the molar extinction coefficient of ICT band in EtOH is very low and different from other solvents like DMSO and H_2O. Hydrophobic and hydrophilic parameters play an important role on solvation and solute-solvent cluster formation with EtOH. Above experimental result can be only explained on the basis of solvation nature and formation of solute-solvent cluster. So, Cluster formation in EtOH is different from DMSO and H_2O solvents and shows low molar extinction coefficient of ICT band.

The O-H Potential Energy Profile

The dissociating O-H bond potential energy profile of HyDC-solvent complex gives the barrier for proton transfer from HyDC to the neighboring solvent molecules. The potential energy profile for dissociating O-H bond of HyDC-DMSO and protonated HyDC-H_2O complex, at ground, is presented in figure 9 from DFT calculation using hybrid functional CAM-B3LYP with 6-311G++ (d, p) basis. The equilibrium bond length of O-H in HyDC is altered from 0.98 Å to 1.00 Å for HyDC-DMSO and HyDC-H_2O complex respectively at ground state.

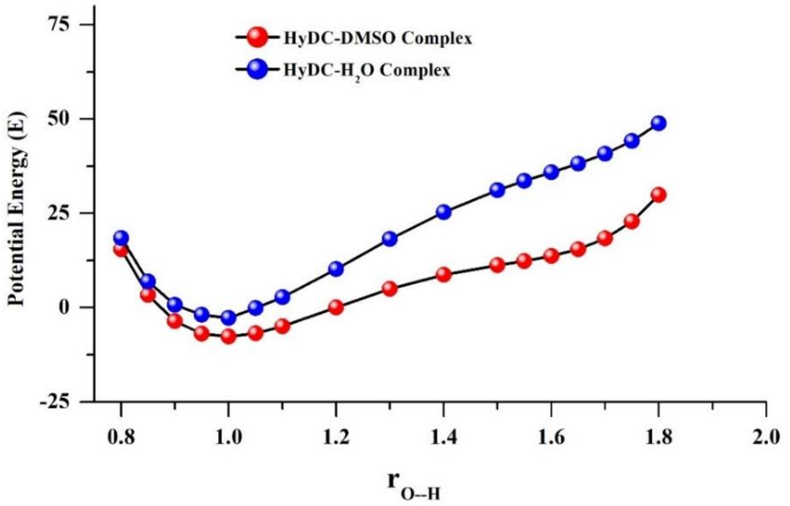

Figure 9: Potential energy curve of HyDC-DMSO and HyDC-H_2O complexes (1:1 complex)

In these cases, it is seen that when the O-H bond distance is increased, the energy decreases and the system become stable up to 1.40 Å. The potential energy profile of the dissociating O−H bond of HyDC at ground state shows a minimum at O-H bond distance ~1.00 Å. Further increasing O-H bond length leads to destabilization of the system. However, rigid potential energy scan of the acidic O-H bond of HyDC-DMSO and HyDC-H_2O complex at ground state reveals that in the presence of solvent molecules, the acidic proton transfer from HyDC to the neighboring solvent molecules becomes a barrierless process, as shown in Figure 9. The potential energy profiles show that a barrier exists for proton transfer from HyDC to solvent molecules from the DFT calculation.

Electronic Properties Calculation

The electronic absorption spectra are calculated using the time-dependent density functional theory (TD-DFT) using hybrid functional CAM-B3LYP with 6-311G++ (d, p) basis and polarizable continuum model (PCM) with ACN as solvent.

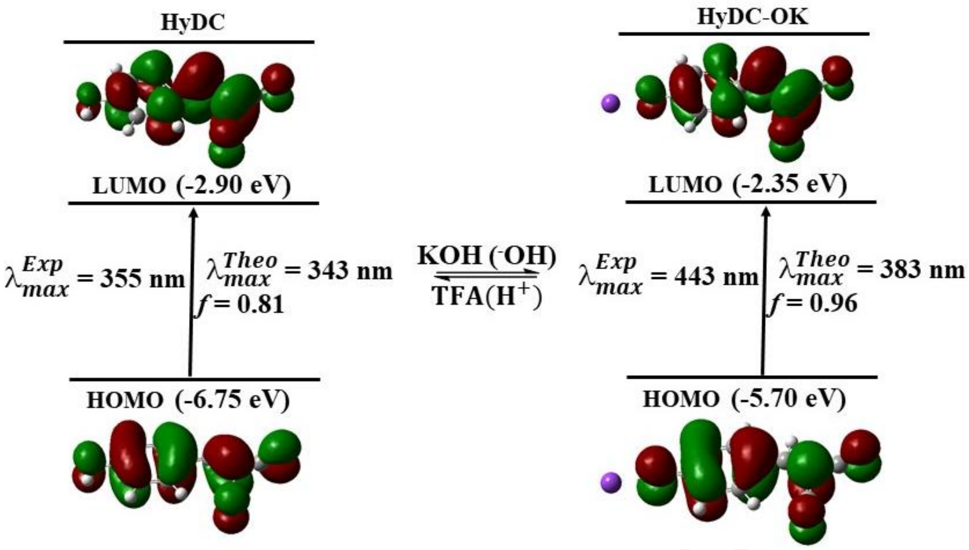

Figure 10: Experimental and theoretical electronic transition of HyDC and HyDC-OK in ACN solvent

It shows the existence of π → π* transition in HyDC and ICT transition in HyDC-OK. The π → π* transition is observed at 354 nm for HyDC due to HOMO to LUMO transition (*f* = 0.81 at 343 nm) (Figure 10). Similarly, ICT transitions are appeared at 443 nm for HyDC-OK due to HOMO to LUMO transition (*f* = 0.96 at 383 nm) respectively and presented in figure 10. Further, time-dependent density functional theory (TD-DFT) using hybrid functional CAM-B3LYP with 6-311G++ (d, p) basis and polarizable continuum model (PCM) with EtOH, H_2O and DMSO as solvent is performed and observed insignificant change of ICT and π → π* transition for both cases. From involvement of orbital in ICT transition process, it can be stated that involvement of benzene π electron with cyano group plays the crucial role for ICT process.

Conclusion

In conclusion, HyDC acts as a strong photoacid and shows highly solvent specific ground state proton transfer process from solute to solvents especially in DMSO and H_2O exclusively. Solvent specific intensity alternation of ICT band in solutions is an indication for ground state proton transfer process. Further, the ground state proton transfer process depends on H-bonding ability of the solvents which is supported by experimental and theoretical studies. In presence of cyano groups (electron withdrawing), the photoacidic nature of HyDC is enhanced and favors the ground state proton transfer (GSPT) process. The solute-solvent interaction is relatively strong and capable of forming microsolvated HyDC clusters with solvents. Strong ICT band in H_2O and DMSO solvents indicates that the ground state proton transfer process is highly feasible due to presence of strong solute-solvent interaction. From above experimental and theoretical results, it can be stated that HyDC acts as a highly active photoacid and ICT probe for monitoring GSPT process.

AUTHOR INFORMATION

Corresponding Author

E-mail: ***sumit.panja@utu.ac.in***; ***sumitkpanja@gmail.com;***

Department of Chemistry, Uka Tarsadia University, Maliba Campus, Gopal Vidyanagar,Bardouli, Mahuba Road, Surat-394350, Gujrat, India.

ORCID of SKP: ***orcid.org/0000-0001-5658-0452***

ACKNOWLEDGMENT

SKP acknowledges to Department of Chemistry, Uka Tarsadia University, Surat-394350, Gujrat, India for providing infrastructure and instrument facilities.

Notes

The authors declare no competing financial interest

References

1. E. A. Meyer, R. K. Castellano, F. Diederich, Interactions with aromatic rings in chemical and biological recognition, Angew. Chem. Int. Ed. 42 (2003) 1210-1250.

2. K. S. Kim, P. Tarakeshwar, J. Y. Lee, Molecular clusters of π-systems: Theoretical studies of structures, spectra, and origin of interaction energies, Chem. Rev. 100 (2000) 4145-4186.
3. B. Brutschy, The structure of microsolvated benzene derivatives and the role of aromatic substituents, Chem. Rev. 100 (2000) 3891-3920.
4. S. K. Panja, S. Verma, S. Saha, Probing phenol dimer in molecular complex: Role of nitro group and stabilizing agent, Journal of Molecular Structure 1193 (2019) 103-109.
5. P. Song, F. -C. Ma, Intermolecular hydrogen-bonding effects on photophysics and photochemistry, Annu. Rev. Phys. Chem. 32 (2013) 589-609.
6. R. Knochenmuss, O. Cheshnovsky, S. Leutwyler, Proton transfer reactions in neutral gas-phase clusters: 1-Naphthol with H_2O, D_2O, CH_3OH, NH_3 and piperidine, Chem. Phys. Lett. 144 (1988) 317-323.
7. T. Förster, Primary photophysical processes. Pure Appl. Chem. 34 (1973) 225-234.
8. O. Gajst, L. P. da Silva, J. C. G. E. da Silva, D. Huppert, Excited-state proton transfer from the photoacid 2-Naphthol-8-sulfonate to acetonitrile/water mixtures, J. Phys. Chem. A 122 (2018) 6166-6175.
9. C. Reichardt, Solvents and solvent effects in organic chemistry; Wiley: 2003.
10. T. Sawamura, A. Fujii, S. Sato, T. Ebata, N. Mikami, Size dependence of intracluster proton transfer of phenol−$(H_2O)_n$ ($n = 1-4$) Cations, J. Phys. Chem. 100 (1996) 8131-8138.
11. J. L. Perez-Lustres, F. Rodriguez-Prieto, M. Mosquera, T. A. Senyushkina, N. P. Ernsting, S. A. Kovalenko, J. Am. Chem. Soc. 129 (2007) 5408-5418.
12. D. K. Deb, B. Sarkar, Theoretical investigation of gas-phase molecular complex formation between 2-hydroxy thiophenol and a water molecule, Phys. Chem. Chem. Phys. 19 (2017) 2466-2478.
13. G.-J. Zhao, K. -Li Han, Hydrogen bonding in the electronic excited state, Acc. Chem. Res. 45 (2012) 404-413.
14. N. Amdursky, Photoacids as a new fluorescence tool for tracking structural transitions of proteins: Following the concentration-induced transition of bovine serum albumin, Phys. Chem. Chem. Phys. 17 (2015) 32023-32032.
15. Excited-state proton transfer of weak photoacids adsorbed on biomaterials: 8-Hydroxy-1,3,6-pyrenetrisulfonate on chitin and cellulose, J. Phys. Chem. A 119 (2015) 1973-1982.

16. Y. Zhang, A. Bendahan, R. Zarbiv, M. P. Kavanaugh, B. I. Kanner, Molecular determinant of ion selectivity of a (Na^++ K^+)-coupled rat brain glutamate transporter, Proc. Natl. Acad. Sci. U. S. A. 95 (1998) 751-755.
17. E. T. Denisov, I. V. Khudyakov, Mechanisms of action and reactivities of the free radicals of inhibitors, Chem. Rev. 87 (1987) 1313-1357.
18. S. K. Panja, S. Saha, Temperature sensor probe based on intramolecular charge transfer (ICT) & reversible solute-solvent interaction in solution, Spectrochimica Acta Part A, 212 (2019) 128-131.
19. S. K. Panja, N. Dwivwdi, S. Saha, Manipulating the proton transfer process in molecular complexes: synthesis and spectroscopic studies, Phys. Chem. Chem. Phys. 18 (2016) 21600-21609.
20. R. Mathew, S. Kayal, A. L.Yapamanu, Excited state structural dynamics of 4-cyano-4′-hydroxystilbene: deciphering the signatures of proton-coupled electron transfer using ultrafast Raman loss spectroscopy, Phys. Chem. Chem. Phys. 21 (2019) 22409-22419.
21. F. Huisken, M. Stemmler, On the structure of the methanol-water dimer, Chem. Phys. Lett. 180 (1991) 332-338.
22. P. A. Stockman, G. A. Blake, F. J. Lovas, R. D. Suenram, Microwave rotation-tunneling spectroscopy of the water–methanol dimer: Direct structural proof for the strongest bound conformation, J. Chem. Phys. 107 (1997) 3782-3790.
23. M. Gerhards, K. Kleinermanns, Structure and vibrations of phenol(H_2O)$_2$, J. Chem. Phys. 103 (1995) 7392-7400.
24. O. Dopfer, M. Fujii, Probing solvation dynamics around aromatic and biological molecules at the single-molecular level, Chem. Rev. 116 (2016) 5432-5463.
25. M. Sugiyama, H. Ishikawa, W. Setaka, M. Kira, N. Mikami, Solvent reorientation process in the “twisted” intramolecular charge-transfer process of cyanophenyldisilane−(H_2O)$_2$ cluster investigated by transient infrared spectroscopy, J. Phys. Chem. A 112 (2008) 1168-1171.
26. R. C. Guedes, B. J. C. Cabral, J. A. M. Simones, H. P. Diogo, Theoretical study of the ionization of phenol−water and phenol−ammonia hydrogen-bonded complexes, J. Phys. Chem. A 104 (2009) 6062-6068.
27. D. Kwasniewski, M. Butler, H. Reisler, Vibrational predissociation of the phenol–water dimer: a view from the water, Phys. Chem. Chem. Phys. 21 (2019) 13968-13976.

28. S. Chaudhuri, A. Acharya, E. T. J. Nibbering, V. S. Batista, Regioselective ultrafast photoinduced electron transfer from naphthols to halocarbon solvents, J. Phys. Chem. Lett. 10 (2019) 2657-2662.
29. H. Yokoyama, H. Watanabe, T. Omi, S. -I. Ishiuchi, M. Fujii, Structure of hydrogen-bonded clusters of 7-azaindole studied by IR dip spectroscopy and ab initio molecular orbital calculation, J. Phys. Chem. A 105 (2001) 9366-9374.
30. P. C. Singh, B. Bandyopadhyay, G. N. Patwari, Structure of the phenylacetylene−water complex as revealed by infrared-ultraviolet double resonance spectroscopy, J. Phys. Chem. A, 112 (2008) 3360-3363.
31. W. Garrett, T. S. Zwier, D. L. Severance, Spectroscopy of mixed-solvent clusters: benzene-water-methanol (C_6H_6-$(H_2O)_n$-$(CH_3OH)_m$), J. Phys. Chem. 96 (1992) 9710-9718.
32. M. Miyazaki, N. Washio, M. Fujii, Electron-proton transfer mechanism of excited-state hydrogen transfer in phenol−$(NH_3)_n$ (n = 5) studied by delayed ionization detected femtosecond time-resolved NIR spectroscopy, Chem. Phys. 515 (2018) 580-585.
33. M. Miyazaki, A. Naito, T. Ikeda, J. Klyne, K. Sakota, H. Sekiya, O. Dopfer, M. Fujii, Real-time observation of the photoionization-induced water rearrangement dynamics in the 5-hydroxyindole–water cluster by time-resolved IR spectroscopy, Phys. Chem. Chem. Phys. 20 (2018) 3079-3091.
34. Y. Matsumoto, T. Ebata, N. Mikami, Characterizations of the hydrogen-bond structures of 2-naphthol-$(H_2O)_n$ (n= 0–3 and 5) clusters by infrared-ultraviolet double-resonance spectroscopy, J. Chem. Phys. 109 (1998) 6303-6311.
35. R. C. Guedes, B. J. Costa Cabral, J. A. Martinho Simoes, H. P. Diogo, Thermochemical properties and structure of phenol−$(H_2O)_{1-6}$ and Phenoxy-$(H_2O)_{1-4}$ by density functional theory, J. Phys. Chem. A 104 (2000) 6062-6068.
36. C. Spies, B. Finkler,a N. Acar, G. Jung, Solvatochromism of pyranine-derived photoacids, Phys. Chem. Chem. Phys. 15 (2013) 19893-19905.
37. G. Jones, Knoevenagel Condensation in Organic Reaction, Wiley, New York, 1967, vol. 15, p. 204.
38. S. P. Tanis, T. T. Parker, J. R. Colca, R. M. Fisher, R. F. Kletzein, Synthesis and Biological Activity of Metabolites of the Antidiabetic, Antihyperglycemic Agent Pioglitazone, J. Med. Chem. 39 (1996) 5053-5063.

39. J. B. Houze, L. Zhu, Y. Sun, M. Akerman, W. Qiu, A. J. Zhang, R. Sharma, M. Schmitt, Y. Wang, J. Liu, J. Liu, J. C. Medina, J. D. Reagan, J. Luo, G. Tonn, J. Zhang, J. Ying-Lin Lu, M. Chen, E. Lopez, K. Nguyen, L. Yang, L. Tang, H. Tian, S. J. Shuttleworth, D. C.-H. Lin, AMG 837: a potent, orally bioavailable GPR40 agonist, Bioorg. Med. Chem. Lett. 22 (2012) 1267-1270.
40. M. K. Tiwari, M. Das, S. Saha, Evidence of CT complex formation between a probe and unreacted methylimidazole in imidazolium cation based ionic liquids: sensing by functionalised 2-benzyledinemalononitrile Analyst 144 (2019) 4432–4438
41. S. K. Panja, N. Dwivedi, S. Saha, First report of the application of simple molecular complexes as organo-catalysts for Knoevenagel condensation, RSC Adv. 5 (2015) 65526-65531.
42. M. J. Frisch et al. GAUSSIAN 09, REVISION D.02, Gaussian, Inc., Wallingford, CT, **2010**.
43. S. K. Panja, N. Dwivwdi, S. Saha, Tuning the intramolecular charge transfer (ICT) process in push–pull systems: effect of nitro groups, RSC Adv. 6 (2016) 105786-105794.
44. H. A. Benesi, J. H. Hildebrand, A spectrophotometric investigation of the interaction of iodine with aromatic hydrocarbons, J. Am. Chem. Soc. 71 (1949) 2703-2707.
45. J. W. Riley, B. Wang, J. L. Woodhouse, M. Assmann, G. A. Worth, H. H. Fielding, Unravelling the role of an aqueous environment on the electronic structure and ionization of phenol using photoelectron spectroscopy, J. Phys. Chem. Lett. 9 (2018) 678-682.
46. P. Krishnakumar, R. Kar, D. K. Maity, Microhydration of 2-naphthol at ground, first excited triplet, and first excited singlet states: A case study on photo acids, J. Phys. Chem. A, 122 (2018**)** 929-936.
47. S. Kaneko, S. Yotoriyama, H. Koda, S. Tobita, Excited-state proton transfer to solvent from phenol and cyanophenols in water, J. Phys. Chem. A 113 (2009) 3021-3028.

Graphical Abstract

Photoacid as ICT Probe for Ground State Proton Transfer Process from Solute to Solvents

Sumit Kumar Panja,*

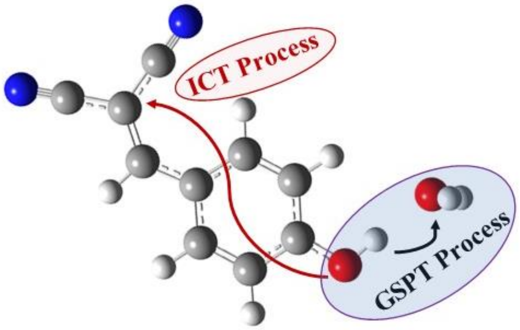

Solvent specific ground state proton transfer (GSPT) process is observed from solute (protoacid; HyDC) to solvents. Protoacid HyDC has shown strong ICT process in solution and used as ICT probe for GSPT process.

Highlights

- ✓ Solvent specific ground state proton transfer (GSPT) process is observed from solute (protoacid; HyDC) to solvents.
- ✓ Protoacid (HyDC) has shown strong ICT process in solution.
- ✓ Protoacid (HyDC) is used ICT probe for GSPT process.

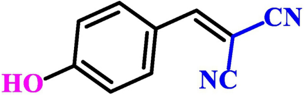

2-(4-Hydroxybenzylidene)malononitrile

(HyDC)

Figure 1

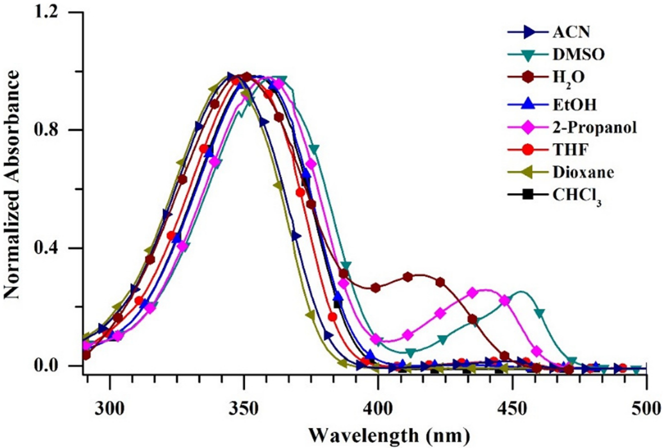
1.2
0.8
0.4
0.0
Normalized Absorbance
300
350
400
450
500
Wavelength (nm)
ACN
DMSO
H_2O
EtOH
2-Propanol
THF
Dioxane
$CHCl_3$

Figure 2

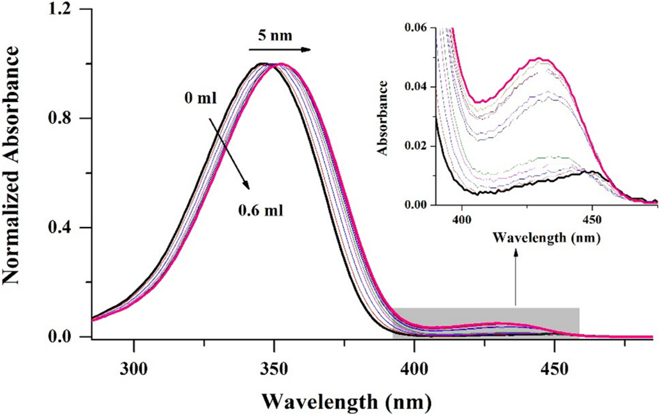

1.2
0.8
0.4
0.0
Normalized Absorbance
5 nm
0 ml
0.6 ml
300
350
400
450
Wavelength (nm)
0.06
0.04
0.02
0.00
Absorbance
400
450
Wavelength (nm)

Figure 3

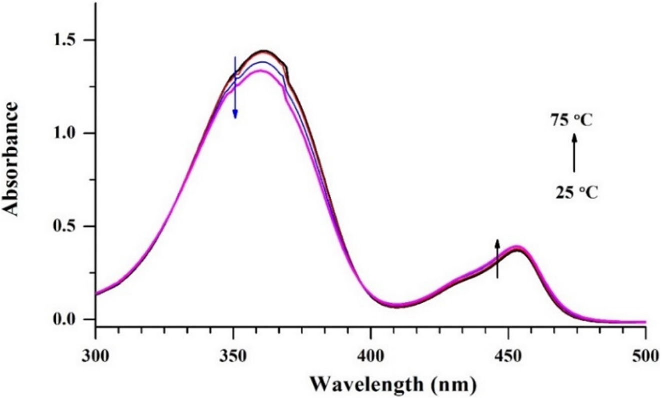
Absorbance
1.5
1.0
0.5
0.0
300
350
400
450
500
Wavelength (nm)
75 °C
25 °C

Figure 4

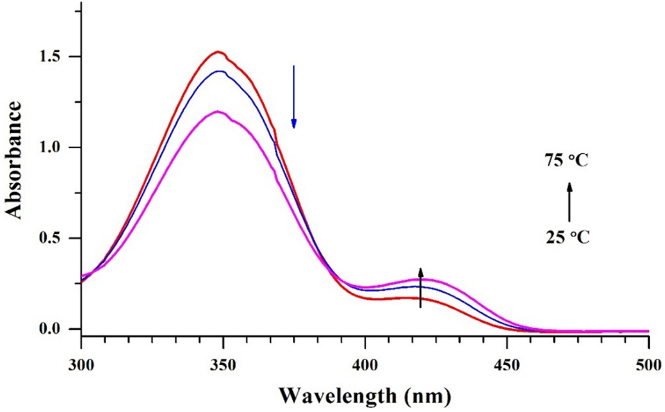
Absorbance
1.5
1.0
0.5
0.0
300
350
400
450
500
Wavelength (nm)
75 °C
25 °C

Figure 5

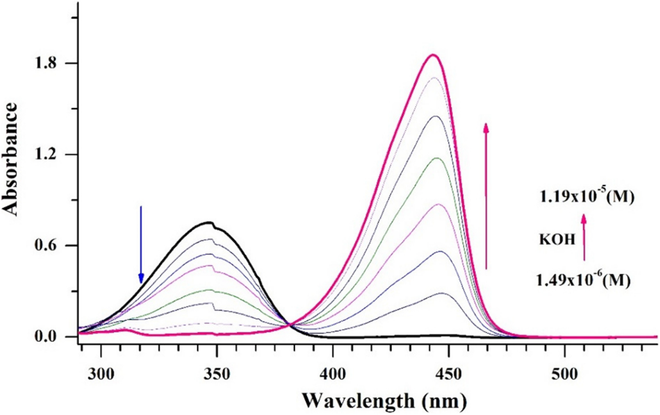
Absorbance
1.8
1.2
0.6
0.0
300
350
400
450
500
Wavelength (nm)
1.19x10^-5(M)
KOH
1.49x10^-6(M)

Figure 6

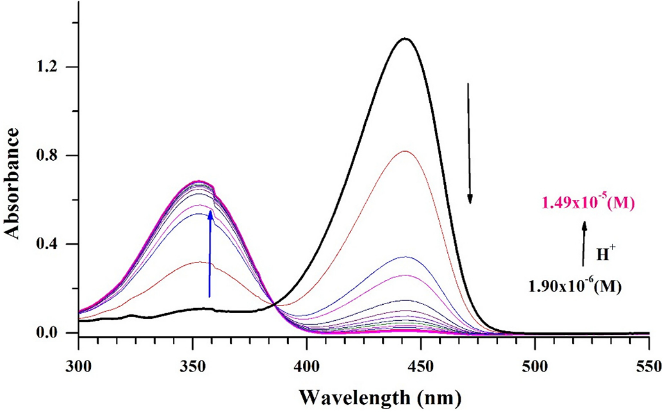
Absorbance
0.0
0.4
0.8
1.2
300
350
400
450
500
550
Wavelength (nm)
1.49x10^-5(M)
H^+
1.90x10^-6(M)

Figure 7

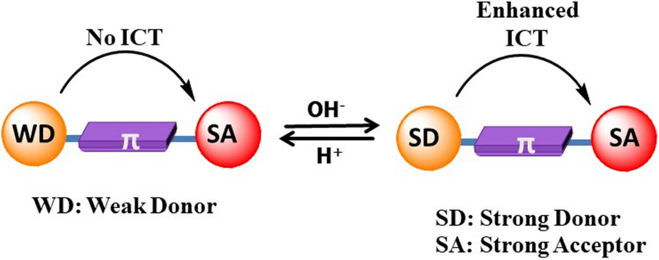
No ICT
WD
π
SA
OH⁻
H⁺
Enhanced ICT
SD
π
SA
WD: Weak Donor
SD: Strong Donor
SA: Strong Acceptor

Figure 8

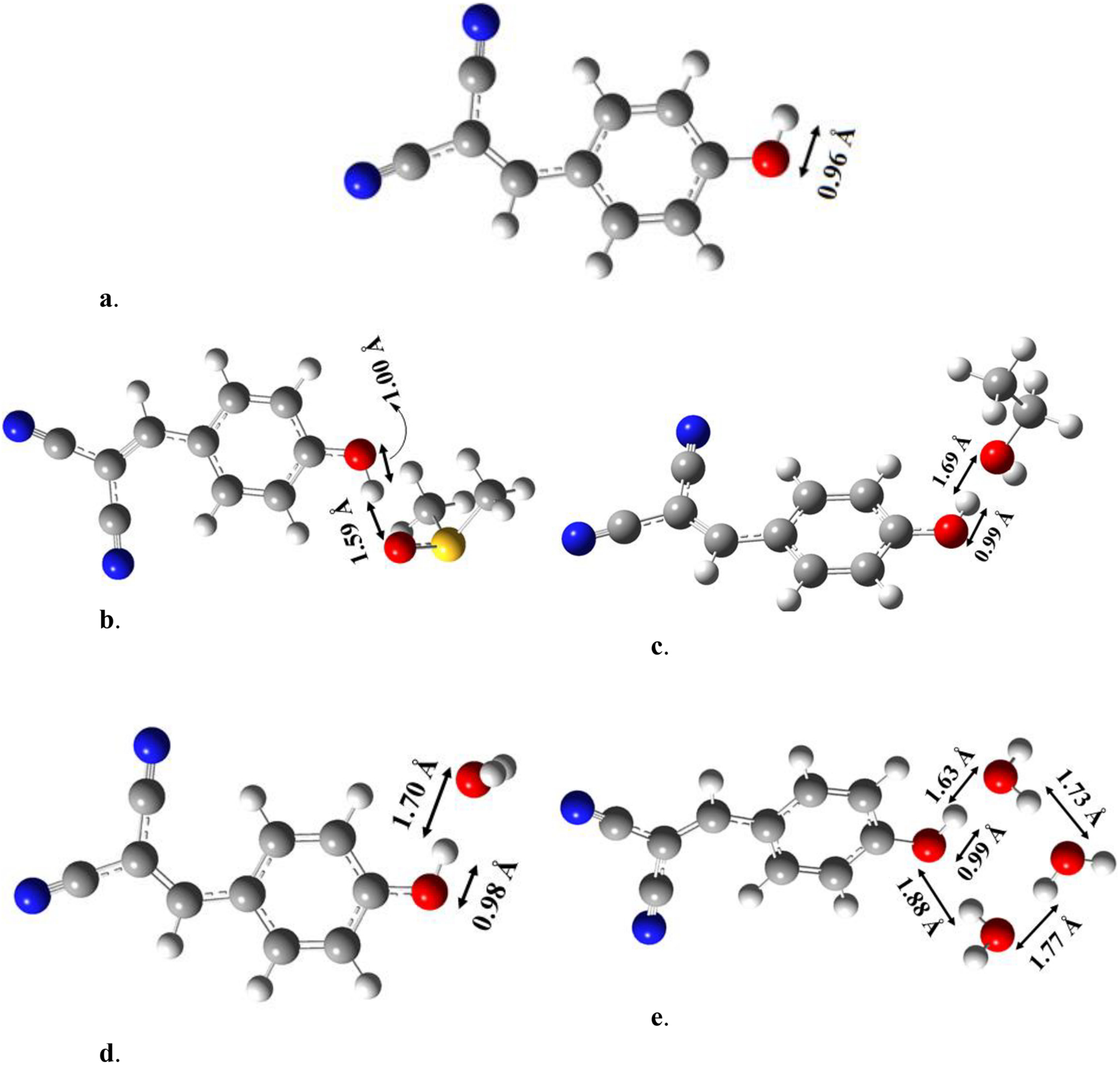
0.96 Å
a.
1.00 Å
1.59 Å
b.
1.69 Å
0.99 Å
c.
1.70 Å
0.98 Å
d.
1.63 Å
1.73 Å
0.99 Å
1.88 Å
1.77 Å
e.

Figure 9

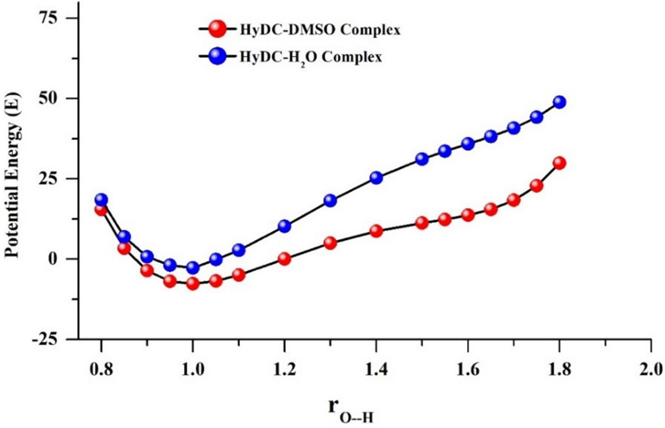
HyDC-DMSO Complex
HyDC-H$_2$O Complex
Potential Energy (E)
75
50
25
0
-25
0.8
1.0
1.2
1.4
1.6
1.8
2.0
$r_{O\text{--}H}$

Figure 10

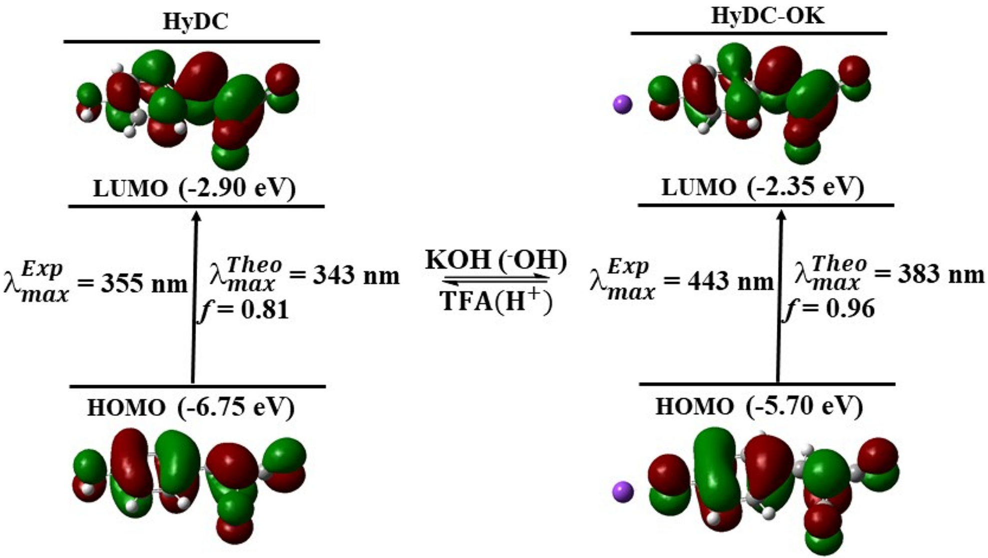
HyDC
LUMO (-2.90 eV)
λ_{max}^{Exp} = 355 nm
λ_{max}^{Theo} = 343 nm
f = 0.81
HOMO (-6.75 eV)
KOH ($^{-}$OH)
TFA(H^{+})
HyDC-OK
LUMO (-2.35 eV)
λ_{max}^{Exp} = 443 nm
λ_{max}^{Theo} = 383 nm
f = 0.96
HOMO (-5.70 eV)

Figure 11